Simultaneous whole-cell patch-clamp and calcium imaging on myenteric neurons

Li, ZL; BOESMANS, Werend; Kazwiny, Y; Hao, MM & Vanden Berghe, P (2022)
Simultaneous whole-cell patch-clamp and calcium imaging on myenteric neurons. In: AMERICAN JOURNAL OF PHYSIOLOGY-GASTROINTESTINAL AND LIVER PHYSIOLOGY, 323 (4) , p. G341 -G347.

DOI: 10.1152/ajpgi.00162.2022
Handle: http://hdl.handle.net/1942/40383

Simultaneous whole-cell patch-clamp and calcium imaging on myenteric neurons

Zhiling Li[1,2], Werend Boesmans[3,4], Youcef Kazwiny[1], Marlene M. Hao[1,5]*, Pieter Vanden Berghe[1,6]*

[1] Laboratory for Enteric Neuroscience (LENS), TARGID, ChroMeta, KU Leuven, Belgium.
[2] Brain Cognition and Brain Disease Institute (BCBDI), Shenzhen Institutes of Advanced Technology, Chinese Academy of Sciences, Shenzhen, China.
[3] Biomedical Research Institute (BIOMED), Hasselt University, Hasselt, Belgium.
[4] Department of Pathology, GROW-School for Oncology and Reproduction, Maastricht University Medical Centre, Maastricht, The Netherlands.
[5] Department of Anatomy and Physiology, the University of Melbourne, Australia.
[6] Leuven Brain Institute (LBI), KU Leuven, Belgium.

* These authors contributed equally to this manuscript. Correspondence to:

Pieter Vanden Berghe: pieter.vandenberghe@kuleuven.be
Laboratory for Enteric Neuroscience
KULeuven, TARGID
Herestraat 49, O&N1, Box 701
3000 Leuven
Belgium

Marlene M. Hao: hao.m@unimelb.edu.au
Department of Anatomy and Physiology, Medical Building
The University of Melbourne
Parkville, VIC
Australia 3010

Abstract

Live calcium imaging is often used as a proxy for electrophysiological measurements and has been a valuable tool that allows simultaneous analysis of neuronal activity in multiple cells at the population level. In the enteric nervous system, there are two main electrophysiological classes of neurons, AH- and S-neurons, which have been shown to have different calcium handling mechanisms. However, they are rarely considered separately in calcium imaging experiments. A handful of studies have shown that in guinea pig, a calcium transient will accompany a single action potential in AH-neurons, but multiple action potentials are required to generate a calcium transient in S-neurons. How this translates to different modes of cellular depolarisation and whether this is consistent across species is unknown. In this study, we used simultaneous whole-cell patch-clamp electrophysiology together with calcium imaging to investigate how enteric neurons respond to different modes of depolarisation. Using both traditional (4Hz) and also high-speed (1000Hz) imaging techniques, we found that single action potentials elicit calcium transients in both AH-neurons and S-neurons. Sub-threshold membrane depolarisations were also able to elicit calcium transients, although calcium responses were generally amplified if an action potential was present. Further, we identified that responses to nicotinic acetylcholine receptor stimulation can be used to distinguish between AH- and S-neurons in calcium imaging.

New and Noteworthy

Live calcium imaging is an important tool for investigating ENS function. Previous studies have shown that multiple action potentials are needed to generate a calcium response in S-neurons, which has important implications for the interpretation of calcium imaging data. Here, we show that in mouse myenteric neurons, calcium transients are elicited by single action potentials in both AH- and S-neurons. In addition, nicotinic acetylcholine receptor stimulation can be used to distinguish between these two classes.

Introduction:

Transmission of neuronal information in a network occurs via action potentials (APs) that travel along the neuronal axon to induce neurotransmitter vesicle release at the synaptic terminal. Although APs are carried by Na^+ ions, they are also accompanied by an influx of Ca^{2+} ions in the cytosol, leading to an overall increase in intracellular Ca^{2+} concentration ($[Ca^{2+}]_i$) (1), which can be readily detected and recorded via fluorescent calcium sensors. In the enteric nervous system (ENS), studies over the past 50 years have shown that there are 2 electrophysiologically distinct subtypes of enteric neurons: AH (after-hyperpolarising) neurons and S (synaptic) neurons (2-4). AH-neurons typically have an "inflection" on the repolarizing phase of their AP (5, 6), followed by a prominent slow after-hyperpolarising potential (sAHP). A key property of these neurons is that their action potential is carried in part by Ca^{2+} ion influx, which underlies the observed inflection point (7). S-neurons are named after the fast excitatory "synaptic" potentials (fEPSPs) that they receive. Although this AH/S classification is derived from guinea pig, it is also used, albeit with adaptations, to subdivide enteric neurons in other species, including mice (8, 9) and humans (10).

The different calcium handling properties of AH and S neurons have been investigated in a handful of studies in the guinea pig (11-14). A calcium transient was found to accompany a single AP in AH-neurons, but multiple action potentials are required to generate a calcium transient in S-neurons. However, how this relates to different forms of neuronal excitation and whether it's consistent across species is unknown. With the increased use of transgenic mice for ENS studies and genetically encoded calcium indicators (such as GCaMPs), understanding how AP firing correlates to the appearance of $[Ca^{2+}]_i$ transients is crucial for the interpretation of calcium imaging data (15, 16).

In the current study, to investigate whether the characteristics of a calcium response could reflect the differences between AH- and S-neurons, we performed simultaneous live calcium imaging and whole-cell patch-clamp electrophysiology on primary cultures of myenteric neurons from *Wnt1|GCaMP6f* mice using different forms of depolarisation.

Materials and Methods:

Animals

For all recordings adult *Wnt1::Cre;R26R-RCL-GCaMP6f* mice (short: *Wnt1|GCaMP6f*) were used, where the genetically-encoded Ca^{2+} indicator, GCaMP6f, is expressed in all neural crest-derived cells, including all cells of the ENS. *Wnt1|GCaMP6f* mice were bred by mating heterozygous *Wnt1::Cre* mice (RRID:MGI:2386570)(17) with homozygous *R26R-RCL-GCaMP6f* mice (Ai95, The Jackson Laboratory, stock #028865; RRID:IMSR_JAX:028865)(18). All mice were sacrificed by cervical dislocation. All experimental procedures were approved by the animal ethics committee of the KU Leuven.

Mouse primary enteric nervous system cultures

The preparation of mouse primary enteric neuron cultures was adapted from previous studies (19). Briefly, the ileum (15-20cm proximal to caecum) of adult male *Wnt1|GCaMP6f* mice (8-12 weeks of age), was removed and flushed using oxygenated Krebs solution. The mucosa, submucosa and circular muscle were removed, leaving the longitudinal muscle with adherent myenteric plexus (LMMP), which was dissociated in collagenase II (2 mg/ml, Worthington) for 1 hr followed by trypsin (0.05%, Gibco) for 7 min. All cells were plated on glass coverslips in neuronal medium (Neurobasal A medium containing 1x B-27, 1 % FBS, 2 mM L-glutamine, 10 ng/ml GDNF and 1% penicillin/streptomycin; Gibco). Cells were cultured for 4-5 days before whole-cell patch clamp and calcium imaging recordings were performed. Recordings were made from a total of 40 cells from 13 animals.

Whole-cell patch-clamp electrophysiology

Cells were visualized on an upright Zeiss Examiner microscope (Axio Examiner.Z1; Carl Zeiss), equipped with a monochromator (Poly V) and cooled CCD camera (Imago QE), both from TILL Photonics. Patch clamp recordings and calcium imaging were performed simultaneously. Cells were superfused with HEPES-buffered saline (in mM: 140 NaCl, 5 KCl, 10 HEPES, 2 $CaCl_2$, 2 $MgCl_2$, and 10 D-glucose, adjusted to pH = 7.4 using NaOH). Patch pipettes were pulled from borosilicate glass capillaries (Harvard Apparatus) using a P-87 puller (Sutter Instruments). Pipette were filled with a potassium methanesulfonate internal solution (in mM: 115 $KMeSO_3$, 9 NaCl, 10 HEPES, 0.1 $CaCl_2$, 1 $MgCl_2$, 0.2 BAPTA.K_4, 2 Mg-ATP, 0.25 Na-GTP and 0.2% biocytin)(20, 21) and had a resistance of approx. 6 MΩ. Pipette capacitance was compensated before whole-cell recording. All recordings were performed at room temperature using a HEKA amplifier and Patchmaster software (both from HEKA Devices, Germany). Liquid junction potentials were calculated using JPCalcW (Molecular Devices) and corrected offline. Data were acquired at 10 kHz and filtered at 2 kHz. All data were analysed using Patchmaster (HEKA) and Igor Pro (Wavemetrics) software. Immediately following whole-cell configuration, current clamp mode was used to measure resting membrane potential (RMP), input resistance (R_{in}), and APs stimulated. Membrane potential was adjusted to approximately -70mV and cells were depolarised by either 10ms or 500ms current pulses in 10pA increments until APs were elicited (rheobase). The amplitude of APs was measured between the baseline membrane potential and the peak of the AP. The 10ms rheobase current was used for combined patch-clamp and calcium imaging recordings. 75mM high K^+ solution was made by substituting the Na^+ component of extracellular solution (in mM: 78 NaCl, 75 KCl, 10 HEPES, 2 $CaCl_2$, 1 $MgCl_2$, and 10 D-glucose, adjusted to pH = 7.4 using NaOH). The agonist dimethylphenylpiperazinium (DMPP; 10 µM; Fluka) and tetrodotoxin (TTX; 1 µM; Sigma) were both diluted in control HEPES-buffered extracellular solution and applied via the inflow. For experiments involving TTX, cells were stimulated 3 times: first in control extracellular solution, a second time in the presence of TTX (1 µM, following a 5 min drug wash-in period), and finally again in control extracellular solution after 5 min washout.

Calcium imaging

GCaMP6f was excited at 470 nm using a Ploychrome V (TILL monochromator), and its fluorescence emission was collected at 525/50 nm using a 20x (NA 1) water dipping objective on an upright Zeiss microscope (Axio Examiner.Z1; Carl Zeiss). Images were captured at a frame rate of 4 Hz. Changes in GCaMP6f fluorescence, reflecting $[Ca^{2+}]_i$ changes, were collected using TILLVISION software (TILL Photonics) and analysis was performed as described previously (22) in Igor Pro using custom written macros (available for download via www.targid.eu > LENS). Regions of interest (ROIs) were drawn, fluorescence intensity for each cell was calculated and normalized to its baseline starting value and presented as F/F_0.

Fast (kHz) calcium imaging

Fast calcium imaging was performed using a CMOS camera (Focuscope SV200-I, Photron; Tokyo, Japan), where images were recorded at a rate of 1000Hz, as described previously (23). During recording, the image intensifier was adjusted to ~550, to yield sufficiently high signal-to-noise ratios, as determined previously (23). Dark noise counts (averaged over 50 dark frames) at an exposure time of 1 ms per image only show a sharp increase above 750 of image intensifier voltage. The read noise, at least up to 750, is also not influenced by the imaging intensifier. All analysis was also performed in Igor Pro (23), updated and complemented by Y. Kazwiny.

Measurement of neuron soma size

The area of neurons was measured from GCaMP6fs images transferred from Igor Pro to ImageJ. A freeform region of interest was drawn around the neuronal soma based on the GCAMP6f fluorescence, and the area calculated.

Data presentation and statistical analysis

All data are presented as mean ± SEM. “n” refers to the number of cells, “N” refers to the number of animals. Statistical analyses were performed with Microsoft Excel or GraphPad. Differences were considered to be significant if $p < 0.05$. All data were analysed using the Students’ *t*-test, unless otherwise stated.

Results and Discussion:

Single action potentials in both AH- and S-neurons trigger calcium transients:

Simultaneous whole-cell patch-clamp and calcium imaging recordings were made from 40 neurons in total, which were randomly selected in cultures. AH neurons were identified by the presence of a hump on the repolarising phase of the AP, which was detected as an inflection in the first derivative of the AP (Figure 1)(5). 16 out of 40 neurons were classified as AH-neurons using this criterion, and the remaining were classified as S-neurons. A prominent slow after-hyperpolarising potential (sAHP) was only observed in 2/16 AH-

neurons (Figure 1), despite using an internal electrode solution that has been shown to promote sAHP detection (21). sAHPs have previously been recorded from AH neurons in *ex vivo* preparations of mouse gut using both sharp electrode recording (8, 24) and whole-cell patch-clamp (21, 25). The lack of a prominent sAHP may be due to differences in cell culture vs the gut environment. Nonetheless, AH-neurons could still be identified using AP shape parameters. Similar to previous studies, AH-neurons identified in our study also exhibited higher capacitance and lower input resistance compared to S-neurons (Table 1)(26).

To stimulate single APs, neurons were stimulated by a short (10ms) depolarising current pulse through the recording electrode. A single AP was able to elicit a $[Ca^{2+}]_i$ transient in the majority of both AH-neurons (*n*=12/15, Figure 1) and S-neurons (*n*=17/23). Interestingly, the amplitude of the AP and the $[Ca^{2+}]_i$ transient were significantly larger for AH- compared to S-neurons (Figure 1). Nonetheless, it appears that a single AP firing will stimulate a $[Ca^{2+}]_i$ transient in both AH- and S- mouse myenteric neurons.

AH-neurons typically fire phasically during a long depolarisation while S-neurons fire tonically (2, 3). In our experiments, both AH- and S-neurons were equally likely to fire either phasically or tonically (Figure 1), which may be due to the lack of a prominent sAHP. While AP amplitude did not differ between the 4 different groups, tonically firing AH neurons had larger $[Ca^{2+}]_i$ transient amplitudes (Figure 1). During tonic AP firing, $[Ca^{2+}]_i$ transients associated with individual APs could not be distinguished using traditional (4Hz) calcium imaging. Hence, we also performed fast imaging of $[Ca^{2+}]_i$ responses (at 1000Hz) combined with simultaneous electrophysiological recording. When multiple APs were elicited by a 500ms depolarisation, individual AP spikes gave rise to step-wise fluorescence changes (Figure 1). However, this was limited by the kinetics of the GCaMP6f calcium indicator used, and steps were detectable if the inter-AP interval was greater than 170ms (*n*=7)(18). Although we did not see any differences in $[Ca^{2+}]_i$ transient amplitude using the fast imaging system, we did observe that the rate of rise of $[Ca^{2+}]_i$ transients appeared to be higher in AH- compared to S-neurons (Figure 1). However, we could only analyse this in *n*=3 AH-neurons, when a single $[Ca^{2+}]_i$ transient corresponding to a single AP could be identified. Therefore, while the $[Ca^{2+}]_i$ transient amplitude is not a reliable method of distinguishing between AH- vs S-neurons, fast imaging of the $[Ca^{2+}]_i$ upstroke may be a useful tool in future studies, particularly if coupled with faster calcium indicators, such as newer generation GCaMPs or synthetic dyes like Fluo4. As such, it can be a valuable addition to voltage-sensitive dye imaging, which has previously been used to investigate enteric neuron activity in a variety of different species (27, 28), to investigate the relation between AP numbers and $[Ca^{2+}]_i$ transient upstroke.

$[Ca^{2+}]_i$ transients are also associated with sub-threshold membrane depolarisations:

To examine the role of the APs in eliciting a $[Ca^{2+}]_i$ transient, we used tetrodotoxin (TTX) to block the majority of voltage-dependent Na^+ channels. TTX abolished all APs and $[Ca^{2+}]_i$

responses produced by 10ms depolarisation (*n*=6/6, Figure 2). Several cells continued to fire an AP in the presence of TTX following 500ms depolarisation (*n*=3/9; APs were identified by the presence of an overshoot above 0mV). A small but detectable $[Ca^{2+}]_i$ transient was identified in all cells, including both AH and S neurons (*n*=9/9, Figure 2). Hence, although $[Ca^{2+}]_i$ transients are elicited by APs, the presence of an AP is not necessary for depolarisation-induced $[Ca^{2+}]_i$ transients, particularly in the case of longer-duration stimuli. Previously, TTX-insensitive APs have been recorded from AH neurons, which were thought to arise from the presence of the additional Ca^{2+} current (4, 7, 29). While the TTX-resistant $Na_v1.9$ channel is also expressed by AH-neurons (30), the slower kinetics of this channel make it unlikely to be responsible for AP conduction (31).

In addition to current pulse depolarisation, we also investigated responses to high extracellular K^+ concentration. We found that although several S-neurons responded to high K^+ with a sub-threshold membrane depolarisation (*n*=5/12), there was no significant difference in $[Ca^{2+}]_i$ responses between AH- and S-neurons (Figure 2).

Nicotinic acetylcholine receptor stimulation can discriminate between AH and S neurons in calcium imaging:

AH neurons rarely exhibit fast excitatory postsynaptic potentials (fEPSPs)(2, 21). As cholinergic-nicotinic transmission is a major mode of fast excitatory neurotransmission in the ENS (32), we investigated how AH neurons identified in our study respond to the nicotinic agonist, DMPP. DMPP did not elicit either a membrane potential change or $[Ca^{2+}]_i$ transient in the majority of AH-neurons (*n*=10/11, Figure 3). In the majority of S-neurons, DMPP triggered a $[Ca^{2+}]_i$ transient and membrane potential change, including either an AP (*n*=7/17, Figure 2) or a sub-threshold depolarisation (*n*=7/17). The $[Ca^{2+}]_i$ amplitude was not different between AP-firing and sub-threshold S-neurons (Figure 3). Three remaining S-neurons did not respond to DMPP. The area of each cell was also examined, and in line with the elevated capacitance, we found that AH neurons were significantly larger than S neurons (Figure 3). Therefore, it appears that the cells least responsive to DMPP identified in our study were larger sized, AH-type neurons, and are therefore, likely to be intrinsic sensory neurons with Dogiel Type-II morphology, i.e. intrinsic primary afferent neurons (IPANs). Although it is possible that some of the activity elicited by DMPP, or indeed also high K^+ application, are indirect responses following synaptic transmission, the sparse nature of these cultures would argue against a major involvement of secondary network activity. Fast imaging and the use of faster calcium sensors will likely help identify direct responding neurons vs secondary responses in future studies. Interestingly, a recent study using *ex vivo* mouse colonic tissue showed that putative intrinsic sensory neurons do receive nicotinic receptor transmission, albeit with reduced responses compared to other neuronal types (33). Whether these reduced responses are amplified *in vitro* requires further investigation.

Conclusions:

Our data show that $[Ca^{2+}]_i$ transients accompany single APs in both AH- and S-type cultured murine enteric neurons. In addition to APs, $[Ca^{2+}]_i$ transients were also elicited by sub-threshold membrane depolarisations, although they were generally amplified if an AP was present. Finally, it appears that the presence of a $[Ca^{2+}]_i$ response to DMPP can be used to optically distinguish between AH- and S-neurons. Our findings will help in the interpretation of calcium imaging data without the need of concurrent electrophysiology recordings. Further integration of neuronal activity recordings with recent transcriptomic data will help understand how the different electrophysiological properties of enteric neurons arise and how it relates to their function.

Table 1: AH- and S-neuronal characteristics

Electrophysiological type	RMP (mV)	R_{in} (MΩ)	C_{in} (pF)	AP amp (mV)	AP half-duration (ms)	Rheobase (pA)	sAHP
AH (n = 16)	-58.0 ± 2.3	346.1 ± 22.7***	17.4 ± 0.9***	93.6 ± 1.9**	2.3 ± 0.04	96.9 ± 9.0**	2/16
S (n = 24)	-58.5 ± 1.6	667.9 ± 55.5***	9.6 ± 0.8***	85.5 ± 1.6**	2.4 ± 0.05	61.3 ± 6.0**	0/24

** Significantly different between AH vs S neurons, $p<0.01$;
*** Significantly different between AH vs S neurons, $p<0.001$; Students' *t*-test

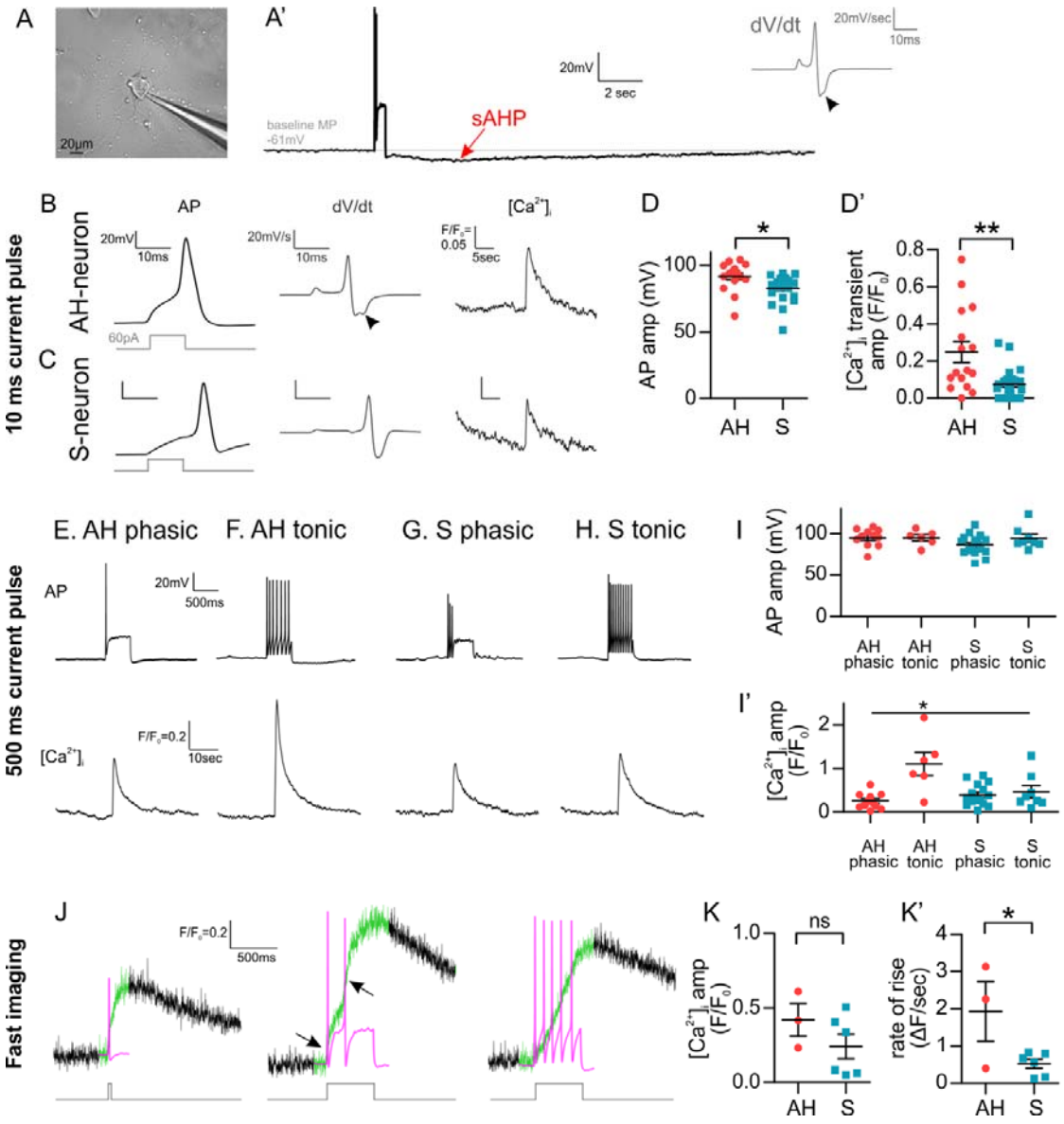

Figure 1: APs and $[Ca^{2+}]_i$ transients in response to current depolarisation using tradition (4Hz, *B-I*) and fast calcium imaging (1000Hz, *J-K*). ***A:*** Brightfield image of myenteric neurons in culture with a patch electrode. ***A':*** Representative trace of an sAHP following action potential firing in an AH-neuron. The derivative of the AP is shown in grey, with an inflection on the repolarising phase (arrowhead). ***B-C:*** Representative traces of responses to 10ms depolarisation in AH *(B)* and S *(C)* neurons. For each recording, the left panel shows the AP (black) with depolarising current pulse (light grey), the middle panel the derivative of the AP (dark grey), and the right panel shows the $[Ca^{2+}]_i$ transient (at a different time scale). An inflection on the repolarising phase can be seen in the first derivative of the AH-neuron (arrowhead). Scale bars in *C* are the same as in *B*. ***D-D':*** Comparison of the AP and $[Ca^{2+}]_i$ transient amplitude in AH- vs. S-neurons (**p*=0.011; ***p*=0.0013; Students' *t*-test; *n*=16 AH neurons, *n*=24 S-neurons). ***E-H:*** Responses to 500ms depolarisation with AP traces shown in top panel and $[Ca^{2+}]_i$ transient shown in lower panel (note differences in time scale between

AP and $[Ca^{2+}]_i$ traces). ***I:*** There were no significant differences between any AH- and S-neurons in AP amplitude following 500ms depolarisation. ***I':*** AH-tonic neurons (*n*=6) exhibited larger $[Ca^{2+}]_i$ amplitudes compared with AH-phasic (*n*=11), S-phasic (*n*=16) and S-tonic (*n*=8; **p*> 0.05; one-way ANOVA, Bonferroni post-hoc test). ***J:*** Fast (1000Hz) calcium imaging with simultaneous whole-cell patch-clamp recordings. Representative traces to 10ms *(left)* and 500ms *(middle, right)* depolarisation with the upstroke of the $[Ca^{2+}]_i$ transient shown in green, and simultaneous AP recordings (magenta) shown on the same time scale. Depolarising current pulses are shown in grey below. In the middle panel, 2 distinct upstrokes of the $[Ca^{2+}]_i$ transient can be observed (arrows), whereas individual events are lost when APs are too close together *(right)*. ***K-K':*** When individual $[Ca^{2+}]_i$ transients to individual APs could be resolved, we observed no significant difference between the $[Ca^{2+}]_i$ transient amplitudes of AH vs S-neurons; however, the $[Ca^{2+}]_i$ transient in AH neurons rose significantly faster (ΔF/time) compared to S-neurons (**p*=0.04, *n*=3 AH-neurons, *n*=6 S-neurons; Students' *t*-test).

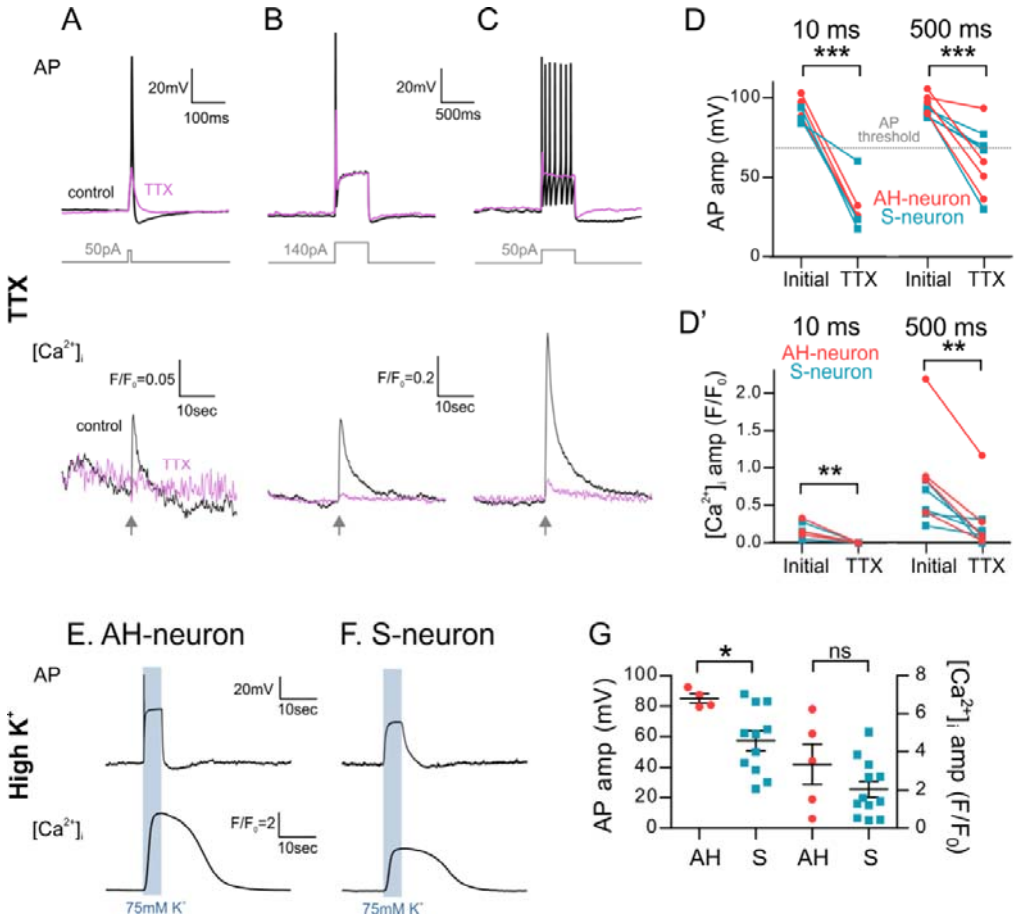

Figure 2: Sub-threshold membrane potential depolarisation and $[Ca^{2+}]_i$ transients following application of TTX *(A-D)*, and in response to high K^+ *(E-G)*. ***A-C:*** Representative traces of APs (top) and corresponding $[Ca^{2+}]_i$ transients (below) to 10ms *(A)* and 500ms *(B-C)* depolarisation before (control, black) and after exposure to TTX (TTX, purple). All traces are from AH neurons. Grey arrow shows the onset of depolarisation for $[Ca^{2+}]_i$ recordings. ***D:*** Comparison of AP amplitude before and after TTX incubation (***p<0.001, n=6 paired t-test). AH and S neurons are represented separately, in red and turquoise, respectively. AP threshold is shown by the dotted grey line, where the membrane potential increased >0 mV. ***D':*** Comparison of $[Ca^{2+}]_i$ transient amplitude before and after TTX incubation (**p<0.01, n=9 paired t-test). TTX abolished 10ms depolarisation-evoked $[Ca^{2+}]_i$ transients, but not 500ms depolarisation-evoked $[Ca^{2+}]_i$ transients in both AH-neurons and S-neurons. ***E-F:*** Representative traces of APs (top) and $[Ca^{2+}]_i$ transients (bottom) in response to high K^+ application. ***G:*** Comparison of AP and $[Ca^{2+}]_i$ transient amplitude in response to high K^+ (*p=0.0284, n=5 AH neurons, n=11 S-neurons; Students' t-test).

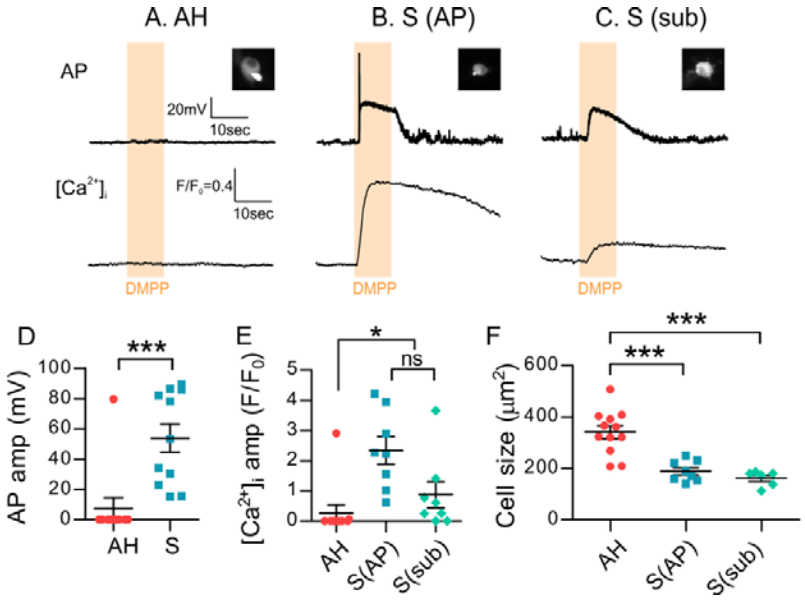

Figure 3: Responses of AH- vs. S-neurons to DMPP. ***A-C:*** Representative traces of APs *(top)* and $[Ca^{2+}]_i$ transients *(bottom)*. The majority of AH-neurons did not respond to DMPP *(A)*, while S-neurons responded with either an AP *(B)* or a sub-threshold membrane depolarisation (sub, *C*). ***D:*** Comparison of AP amplitude (***p=0.0008, Students' t-test). ***E:*** Comparison of $[Ca^{2+}]_i$ transient amplitude (*p=0.011; ns: p>0.05; one-way ANOVA). ***F:*** Comparison of sizes of different neurons responding to DMPP (***p<0.001, one-way ANOVA).

References:

1. **Bean BP**. The action potential in mammalian central neurons. *Nature Reviews Neuroscience* 8: 451-465, 2007.
2. **Hirst GDS, Holman ME, and Spence I**. Two types of neurones in the myenteric plexus of duodenum in the guinea-pig. *J Physiol (Lond)* 236: 303-326, 1974.
3. **Bornstein JC, Furness JB, and Kunze WAA**. Electrophysiological characterization of myenteric neurons: how do classification schemes relate? *Journal of the Autonomic Nervous System* 48: 1-15, 1994.
4. **Nishi S, and North RA**. Intracellular recording from myenteric plexus of guinea-pig ileum. *J Physiol (Lond)* 231: 471-491, 1973.
5. **Clerc N, Furness JB, Bornstein JC, and Kunze WAA**. Correlation of electrophysiological and morphological characteristics of myenteric neurons of the duodenum in the guinea-pig. *Neuroscience* 82: 899-914, 1998.
6. **Iyer V, Bornstein JC, Costa M, Furness JB, Takahashi Y, and Iwanaga T**. Electrophysiology of guinea pig myenteric neurons correlated with immunoreactivity for calcium-binding proteins. *Journal of the Autonomic Nervous System* 22: 141-150, 1988.
7. **Hirst GD, Johnson SM, and van Helden DF**. The calcium current in a myenteric neurone of the guinea-pig ileum. *J Physiol (Lond)* 361: 297-314, 1985.
8. **Nurgali K, Stebbing MJ, and Furness JB**. Correlation of electrophysiological and morphological characteristics of enteric neurons in the mouse colon. *J Comp Neurol* 468: 112-124, 2004.
9. **Ren J, Bian X, DeVries M, Schnegelsberg B, Cockayne DA, Ford APDW, and Galligan JJ**. $P2X_2$ subunits contribute to fast synaptic excitation in myenteric neurons of the mouse small intestine. *J Physiol (Lond)* 552: 809-821, 2003.
10. **Carbone SE, Jovanovska V, Nurgali K, and Brookes SJ**. Human enteric neurons: morphological, electrophysiological, and neurochemical identification. *Neurogastroenterol Motil* 26: 1812-1816, 2014.
11. **Vanden Berghe P, Kenyon JL, and Smith TK**. Mitochondrial Ca^{2+} Uptake Regulates the Excitability of Myenteric Neurons. *J Neurosci* 22: 6962-6971, 2002.
12. **Shuttleworth CWR, and Smith TK**. Action potential-dependent calcium transients in myenteric S neurons of the guinea-pig ileum. *Neuroscience* 92: 751-762, 1999.
13. **Tatsumi H, Hirai K, and Katayama Y**. Measurement of the intracellular calcium concentration in guinea pig myenteric neurons by using Fura-2. *Brain Research* 451: 371-375, 1988.
14. **Hillsley K, Kenyon JL, and Smith TK**. Ryanodine-Sensitive Stores Regulate the Excitability of AH Neurons in the Myenteric Plexus of Guinea-Pig Ileum. *J Neurophysiol* 84: 2777-2785, 2000.
15. **Spencer NJ, and Hu H**. Enteric nervous system: sensory transduction, neural circuits and gastrointestinal motility. *Nat Rev Gastroenterol Hepatol* 17: 338-351, 2020.
16. **Boesmans W, Hao MM, and Vanden Berghe P**. Optogenetic and chemogenetic techniques for neurogastroenterology. *Nat Rev Gastroenterol Hepatol* 15: 21-38, 2018.
17. **Danielian PS, Muccino D, Rowitch DH, Michael SK, and McMahon AP**. Modification of gene activity in mouse embryos in utero by a tamoxifen-inducible form of Cre recombinase. *Current Biology* 8: 1323-1326, 1998.
18. **Chen TW, Wardill TJ, Sun Y, Pulver SR, Renninger SL, Baohan A, Schreiter ER, Kerr RA, Orger MB, Jayaraman V, Looger LL, Svoboda K, and Kim DS**. Ultrasensitive fluorescent proteins for imaging neuronal activity. *Nature* 499: 295-300, 2013.

19. **Lowette K, Tack J, and Vanden Berghe P**. Role of corticosterone in the murine enteric nervous system during fasting. *Am J Physiol - Gastrointest Liver Physiol* 307: G905-G913, 2014.
20. **Hao MM, Lomax AE, McKeown SJ, Reid CA, Young HM, and Bornstein JC**. Early Development of Electrical Excitability in the Mouse Enteric Nervous System. *J Neurosci* 32: 10949-10960, 2012.
21. **Mao YK, Wang BX, and Kunze W**. Characterization of myenteric sensory neurons in the mouse small intestine. *J Neurophysiol* 96: 998-1010, 2006.
22. **Boesmans W, Martens MA, Weltens N, Hao MM, Tack J, Cirillo C, and Vanden Berghe P**. Imaging neuron-glia interactions in the enteric nervous system. *Front Cell Neurosci* 7: 2013.
23. **Martens MA, Boesmans W, and Vanden Berghe P**. Calcium imaging at kHz frame rates resolves millisecond timing in neuronal circuits and varicosities. *Biomed Opt Express* 5: 2648-2661, 2014.
24. **Neylon CB, Nurgali K, Hunne B, Robbins HL, Moore S, Chen MX, and Furness JB**. Intermediate-conductance calcium-activated potassium channels in enteric neurones of the mouse: pharmacological, molecular and immunochemical evidence for their role in mediating the slow afterhyperpolarization. *Journal of Neurochemistry* 90: 1414-1422, 2004.
25. **Mao Y-K, Kasper DL, Wang B, Forsythe P, Bienenstock J, and Kunze WA**. Bacteroides fragilis polysaccharide A is necessary and sufficient for acute activation of intestinal sensory neurons. *Nat Commun* 4: 1465, 2013.
26. **Rugiero F, Gola M, Kunze WAA, Reynaud JC, Furness JB, and Clerc N**. Analysis of whole-cell currents by patch clamp of guinea-pig myenteric neurones in intact ganglia. *J Physiol (Lond)* 538: 447-463, 2002.
27. **Mazzuoli G, and Schemann M**. Multifunctional rapidly adapting mechanosensitive enteric neurons (RAMEN) in the myenteric plexus of the guinea pig ileum. *J Physiol (Lond)* 587: 2009.
28. **Michel K, Krüger D, Schäuffele S, Zeller F, Demir IE, Theisen J, and Schemann M**. Fast synaptic excitatory neurotransmission in the human submucosal plexus. *Neurogastroenterol Motil* 33: e14164, 2021.
29. **Hirst GDS, and Spence I**. Calcium action potentials in mammalian peripheral neurons. *Nature New Biol* 243: 54-56, 1973.
30. **Rugiero F, Mistry M, Sage D, Black JA, Waxman SG, Crest M, Clerc N, Delmas P, and Gola M**. Selective Expression of a Persistent Tetrodotoxin-Resistant Na^+ Current and $Na_V1.9$ Subunit in Myenteric Sensory Neurons. *J Neurosci* 23: 2715-2725, 2003.
31. **Coste B, Osorio N, Padilla F, Crest M, and Delmas P**. Gating and modulation of presumptive NaV1.9 channels in enteric and spinal sensory neurons. *Mol Cell Neurosci* 26: 123-134, 2004.
32. **Galligan JJ**. Ligand-gated ion channels in the enteric nervous system. *Neurogastroenterol Motil* 14: 611-623, 2002.
33. **Hibberd TJ, Travis L, Wiklendt L, Costa M, Brookes SJH, Hu H, Keating DJ, and Spencer NJ**. Synaptic activation of putative sensory neurons by hexamethonium-sensitive nerve pathways in mouse colon. *Am J Physiol Gastrointest Liver Physiol* 314: G53-g64, 2018.

Acknowledgements:

We would like to thank the members of the Laboratory for Enteric Neuroscience for their support on this work, particular Mr Michael Moons for his help with animal maintenance and cell culture.

Grant Support:

This study was funded by the Research Foundation Flanders (FWO: G.0921.15) and Hercules foundation (AKUL/11/37 and AKUL/13/37) to PVB. ZL was funded by the China Scholarship Council (CSC: 201408370078) PhD scholarship; MMH is a FWO (12G1214N), Australian National Health and Medical Research Council (NHMRC: APP1655567) and Australian Research Council (ARC: DE190101209) fellow; WB is supported by the Francqui Foundation and grants from the FWO (G036320N) and the Dutch Research Council (NWO VIDI: 016.196.367).

Contribution:

PVB, MMH and WB designed experiments. ZL performed experiments and analysed data. ZL and YK analysed fast imaging data. ZL and MMH drafted the manuscript, which was finalised by all authors.

Disclosures:

The authors have no conflicts to disclose.

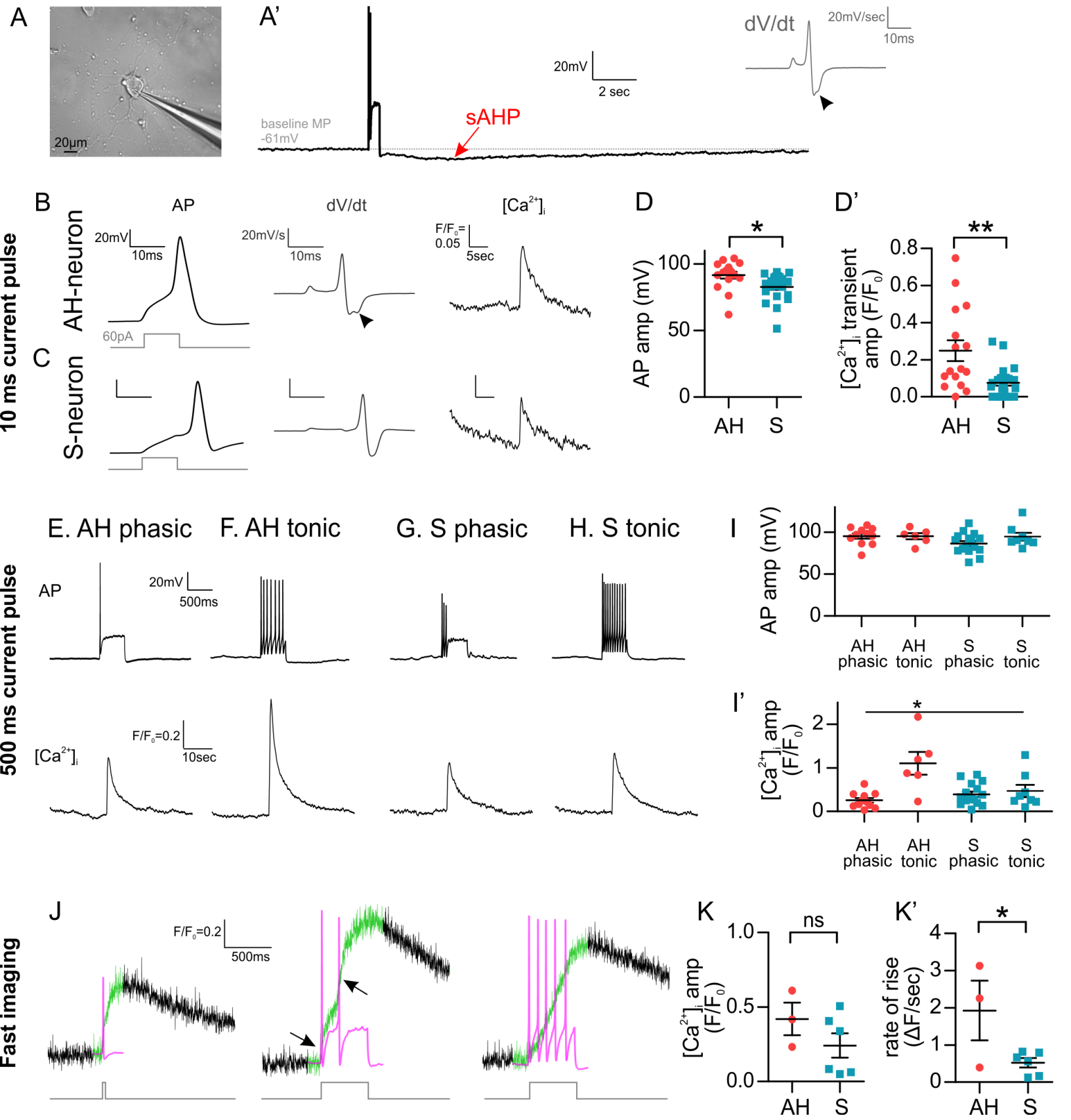
A
20μm
A'
20mV
2 sec
baseline MP
-61mV
sAHP
dV/dt
20mV/sec
10ms
10 ms current pulse
B
AP
dV/dt
[Ca2+]i
AH-neuron
20mV
10ms
20mV/s
10ms
F/F0=
0.05
5sec
60pA
C
S-neuron
D
AP amp (mV)
100
50
0
*
AH
S
D'
[Ca2+]i transient amp (F/F0)
0.8
0.6
0.4
0.2
0.0
**
AH
S
500 ms current pulse
E. AH phasic
F. AH tonic
G. S phasic
H. S tonic
AP
20mV
500ms
[Ca2+]i
F/F0=0.2
10sec
I
AP amp (mV)
100
50
0
AH phasic
AH tonic
S phasic
S tonic
I'
[Ca2+]i amp (F/F0)
2
1
0
*
AH phasic
AH tonic
S phasic
S tonic
Fast imaging
J
F/F0=0.2
500ms
K
[Ca2+]i amp (F/F0)
1.0
0.5
0.0
ns
AH
S
K'
rate of rise (ΔF/sec)
4
3
2
1
0
*
AH
S

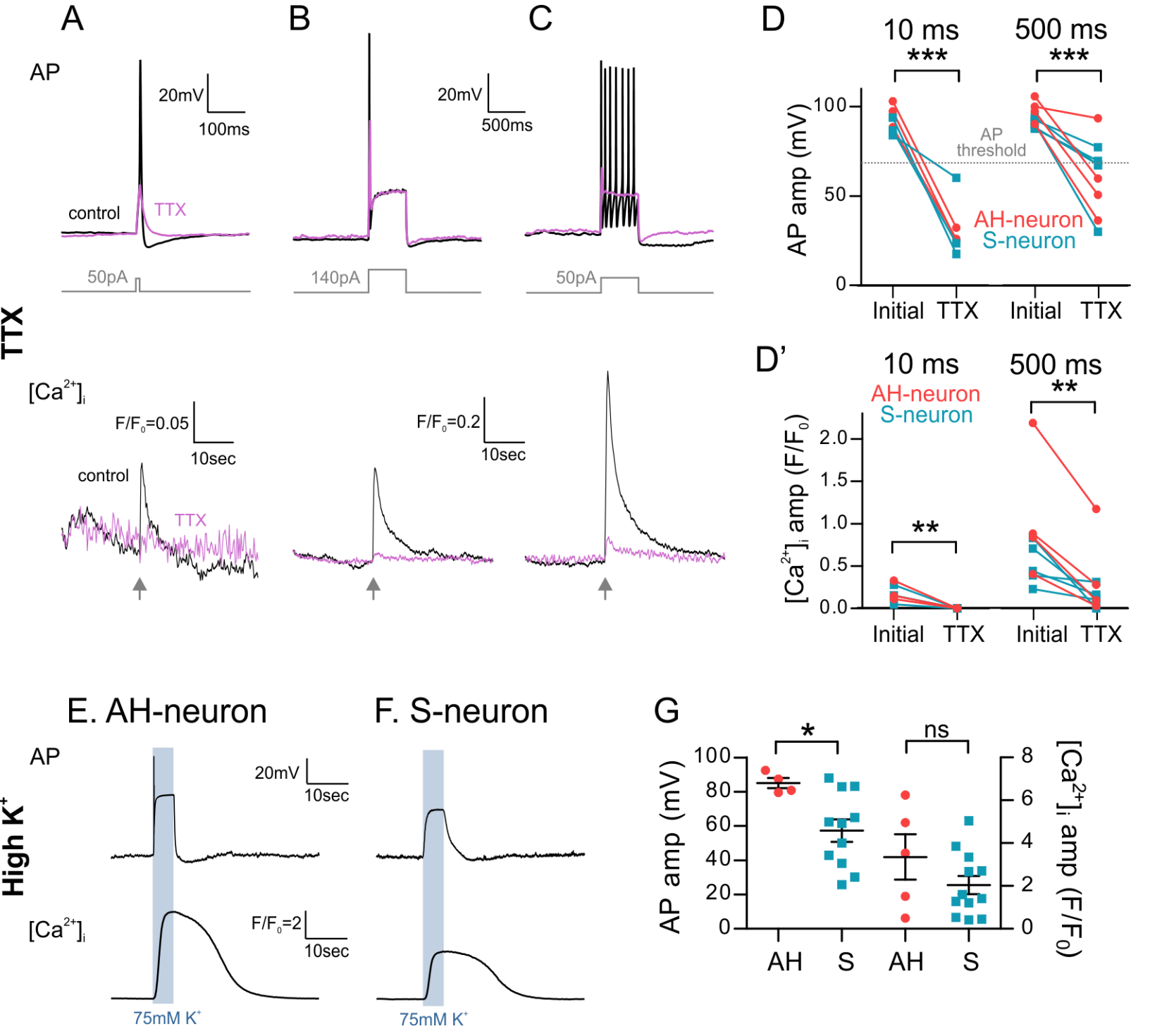
A
B
C
D
AP
20mV
100ms
control
TTX
50pA
20mV
500ms
140pA
50pA
10 ms
500 ms
***
***
AP amp (mV)
100
50
0
AP threshold
AH-neuron
S-neuron
Initial
TTX
Initial
TTX
TTX
[Ca2+]i
F/F0=0.05
10sec
control
TTX
F/F0=0.2
10sec
D'
10 ms
500 ms
AH-neuron
S-neuron
**
**
[Ca2+]i amp (F/F0)
2.0
1.5
1.0
0.5
0.0
Initial
TTX
Initial
TTX
E. AH-neuron
F. S-neuron
G
High K+
AP
20mV
10sec
[Ca2+]i
F/F0=2
10sec
75mM K+
75mM K+
*
ns
AP amp (mV)
100
80
60
40
20
0
[Ca2+]i amp (F/F0)
8
6
4
2
0
AH
S
AH
S

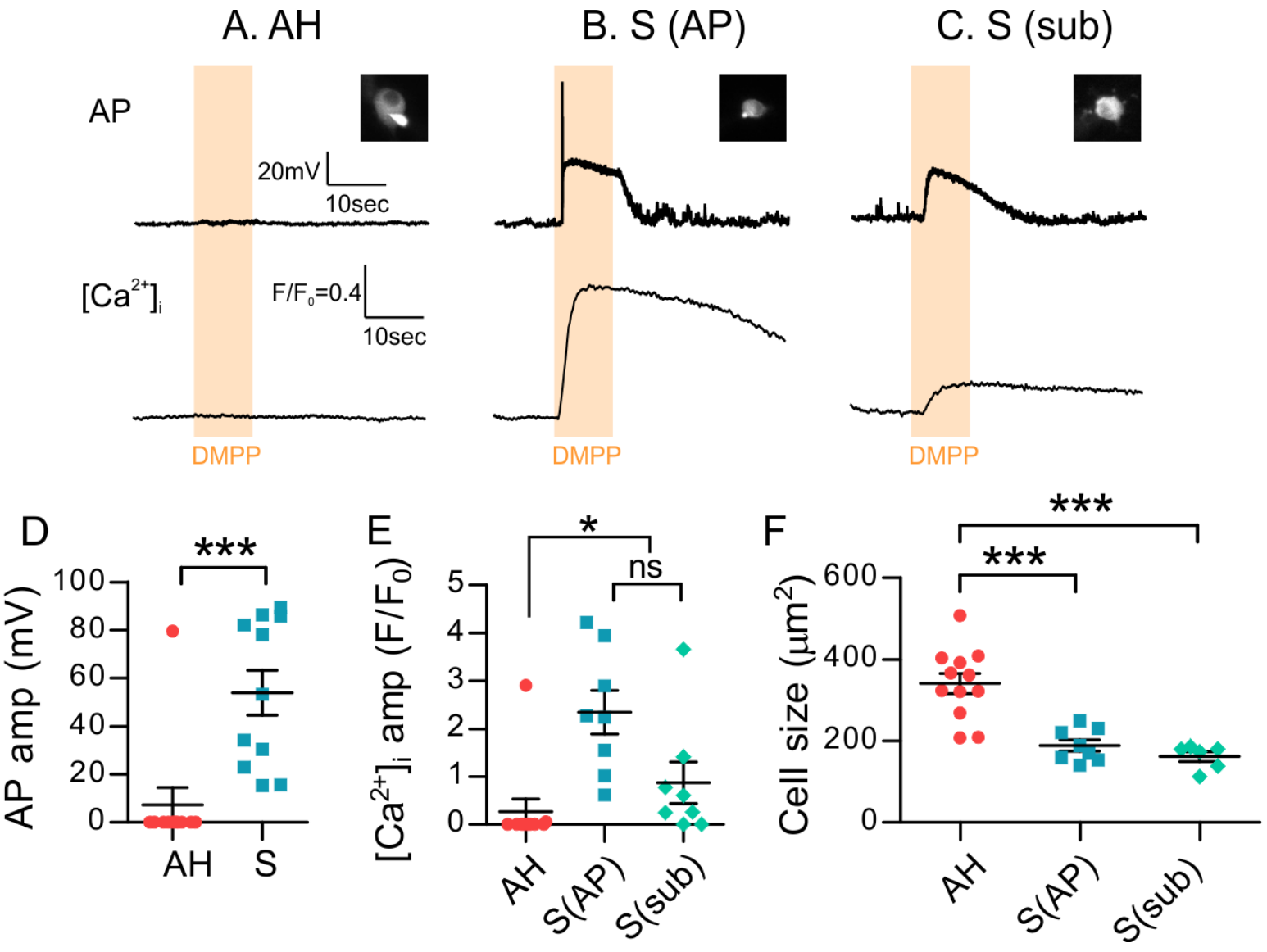
A. AH
B. S (AP)
C. S (sub)
AP
20mV
10sec
[Ca2+]i
F/F0=0.4
10sec
DMPP
DMPP
DMPP
D
AP amp (mV)
***
AH
S
E
[Ca2+]i amp (F/F0)
*
ns
AH
S(AP)
S(sub)
F
Cell size (μm2)
***
***
AH
S(AP)
S(sub)

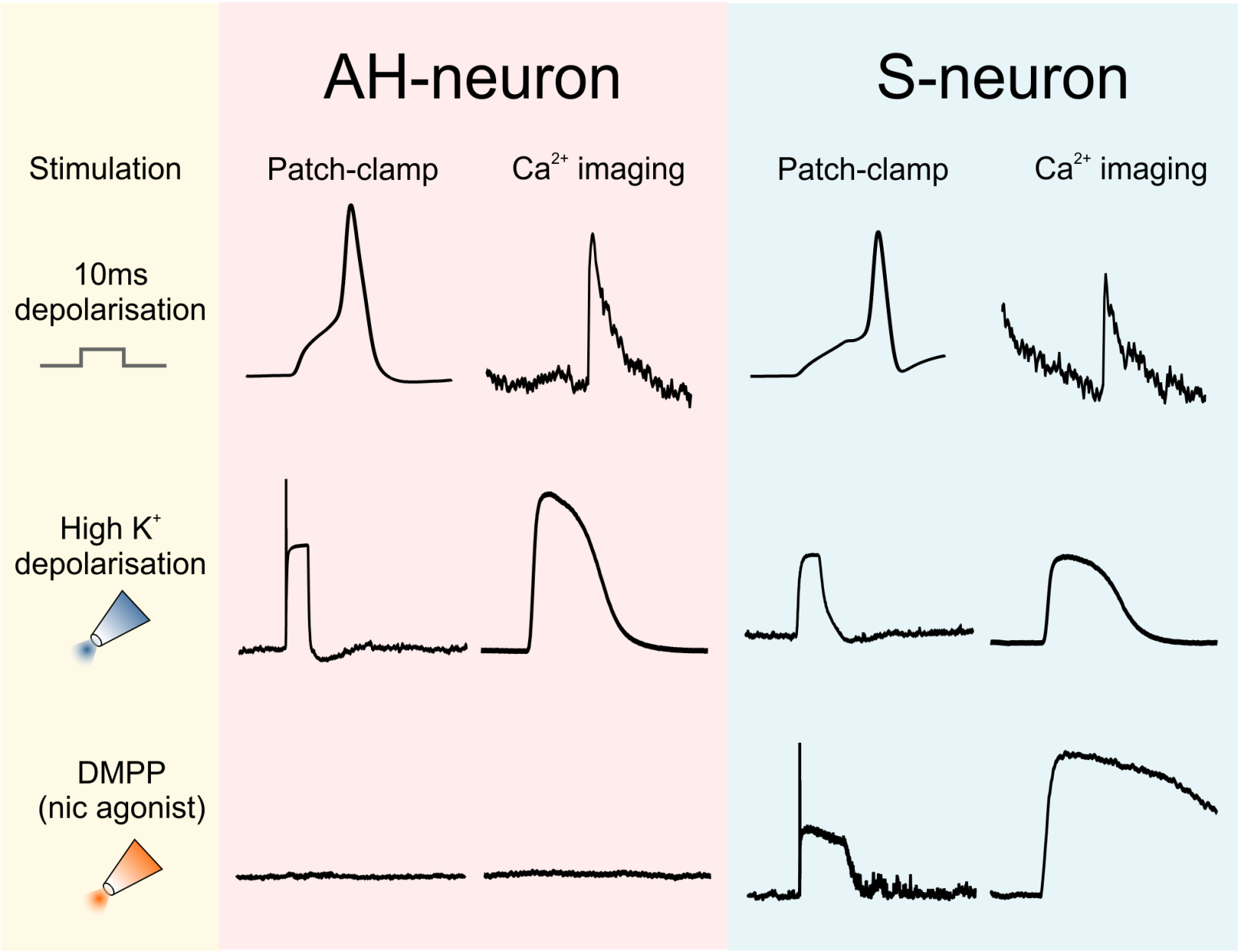
AH-neuron
S-neuron
Stimulation
Patch-clamp
Ca2+ imaging
Patch-clamp
Ca2+ imaging
10ms
depolarisation
High K+
depolarisation
DMPP
(nic agonist)